Robust optimization of nonlinear energy sinks used for mitigation of friction-induced limit cycle oscillations

Cherif Snoun, Baptiste Bergeot, Sébastien Berger

Robust optimization of nonlinear energy sinks used for mitigation of friction-induced limit cycle oscillations

Cherif Snoun, Baptiste Bergeot, Sébastien Berger

INSA CVL, Univ. Orléans, Univ. Tours, LaMé EA 7494, F-41034, 3 Rue de la Chocolaterie, CS 23410, 41034 Blois Cedex, France

Abstract

This paper aims at proposing robust methods to optimize nonlinear energy sinks (NES) used for the mitigation of friction-induced vibrations due to mode coupling instabilities. The study is based on a mechanical system composed of two NES coupled to the well-known two-degrees-of-freedom Hultèn's model. In such an unstable system coupled with NES, it is usual to observe a discontinuity in the steady-state amplitude profile which separates the parameter space into two parts corresponding respectively to the mitigated and unmitigated regimes. The discontinuity is predicted by a methodology previously developed by the authors and based on Multi-Element generalized Polynomial Chaos. The method allows to determine the Propensity of the system to undergo a Harmless Steady-State Regime (PHSSR). The objective of the present work is therefore to maximize the value of the PHSSR to obtain a robust optimal design of the NES. To this end, several stochastic optimization problems are presented that take into account the dispersion of the uncertain parameters using two approaches; in the first one, the parameters of the NES are considered as deterministic, and in the second one they are also supposed uncertain but with a known probability law.

Keywords: Friction-induced vibration, Nonlinear Energy Sink, Uncertainty, Robust optimisation, Polynomial Chaos

1. Introduction

Friction-induced vibrations rank among the major issues that friction systems may face. This phenomenon can result from the generation of Limit Cycle Oscillations (LCO) induced by dry friction, which are explained by the coupling of two modes of the system (Oden and Martins (1985); Fritz et al. (2007); Hervé et al. (2008)). Given the parametric uncertainties present in friction systems, it is very difficult to design them so that they always have stable behaviors. It is therefore necessary to use strategies to attenuate vibrations when they appear. As a way to model this phenomenon, the well-known two-degrees-of-freedom Hultèn's model (Hultén (1997, 1993)) has been widely used in the past.

Nonlinear Energy Sinks (NES) are nonlinear passive vibration absorbers which consist in a spring mass damper with a strong nonlinear stiffness (usually cubic as is the case in this work). The NES can adapt themselves to the Primary Structure (PS) without being tuned to a specific frequency. Their operation is based on the concept of Targeted Energy Transfer (TET) which has become an important passive control technique for reducing or eliminating unwanted vibrations Vakakis and Gendelman (2001); Vakatis et al. (2008). The design and optimization of NES constitute a very dynamic field of research. Recently, a lot of work has for example been produced concerning the study of new configurations and technologies allowing/enhancing TET (Tian et al. (2021); Xiong et al. (2021)), the analysis of the underlying dynamics of the coupled system (Bergeot (2021); Habib and Romeo (2021); Bergeot et al. (2020)), the deterministic optimization of NES (Geng et al. (2021); Khazaee et al. (2019)), the stochastic optimization of NES Pidaparthi and Missoum (2018, 2019), the coupling of the NES to an energy harvester (Fang et al. (2021); Karama et al. (2021); Karličić et al. (2021)) or the use of a NES as an energy harvester (Zhou et al. (2014); Li and Li (2021)), etc. Among the many research subfields about NES, the present work takes place within the framework of robust optimization of NES when the latter have uncertain parameters and are used to mitigate Limit Cycle Oscillations (LCO).

The mitigation of LCO by NES has also been widely studied in the past. The first work reported in this framework concerns the LCO mitigation of the Van der Pol oscillator (Lee et al. (2006)). In the field of friction-induced vibrations mitigation, Bergeot et al. (2017) analyzed the behavior of a Hultèn's model coupled to two ungrounded NES; the same model in considered in this work.

Lately, special attention has been paid to the optimal design of NES in a deterministic context. Nguyen and Pernot (2011) have studied the effectiveness of a NES to attenuate free oscillations of a single degree-of-freedom oscillator. The optimization procedure consisted in studying the influence of the NES damping on the efficiency of the energy transfer from the primary system to the NES. Wang et al. (2019) presented multi-objective designs of a track NES and a single-sided vibro-impact track NES used as

effective control devices to mitigate the seismic response of high-rise buildings. In Qiu et al. (2019) a design criteria for optimally tuned Vibro-Impact NES to control vibration under periodic and transient excitation has been proposed. Oliva et al. (2017) developed an approximate design approach based on the use of the Statistical Linearization Technique, and an accurate empirical formulation linking the NES optimal parameters to the characteristics of the main structure and the random excitation.

More recently, the optimization of NES under uncertainties has also been considered. Boroson (2015) has introduced the "discontinuity in the effectiveness" of the NES, i.e., the fact that the effectiveness can change from a high value to a low value following a small perturbation of the design parameters or of the initial conditions. In Boroson et al. (2017), the optimal design of several parallel NES configurations for maximum mean efficiency has been investigated. It has been shown again that the variation of some system parameters or of the initial conditions generates a discontinuity on the energy shape of the system. An optimization algorithm based on the Support Vector Machine (SVM) technique and a kriging meta-model have been used to predict this discontinuity according to the dispersion of some uncertain parameters. Khazaee et al. (2019) studied the stochastic optimization of multiple NES (configured in parallel and in series) attached to a simply supported pipe conveying fluid. The results show that the optima obtained from stochastic optimization are much more robust than those obtained from deterministic optimization. Pidaparthi and Missoum (2018, 2019) performed optimization of NES under uncertainties in the context of attenuating self-sustained vibrations of an aircraft wing created by aeroelastic instability (which is also due to mode coupling). Depending on the nonlinear properties of the system, the latter may undergo LCO that are either supercritical or subcritical. In this case the bifurcation diagram of the system (which represents the amplitude of the LCO as a function of the airflow velocity over the wing) may exhibit two types of discontinuities, respectively due to the operation of the NES, and to the generation of subcritical LCO. Using again the SVM technique and a kriging meta-model, several stochastic optimization problems have been presented in order to maximize the average reduction of the LCO amplitude.

Various probabilistic approaches may be used to study the propagation of uncertainties in the deterministic model (DM) of a mechanical system. A review of the numerical methods dedicated to the stochastic prediction can be found in Nouy (2009). Efficient methods such as the generalized Polynomial Chaos (gPC) or the Multi-Element generalized Polynomial Chaos (ME-gPC) have been developed as a less costly alternative to the common Monte Carlo approach. These methods have been for example used to perform a stochastic analysis of the dynamic behavior of friction systems (Nechak et al. (2011, 2012, 2013, 2018); Sarrouy et al. (2012, 2013); Trinh et al. (2016); Snoun et al. (2020)).

In this paper, two original optimization methods under uncertainties, based on polynomial chaos theory, are developed for the robust design of two ungrounded NES used to mitigate LCO due to mode coupling instability in the Hultèn's model, which is the primary structure (PS). Bergeot et al. (2017) classified the steady-state response regimes in two main categories related to the dispersion of some uncertain parameters: the mitigated regimes (harmless situations) and the unmitigated regimes (harmful situations). In the context of instability mitigation by means of NES, the LCO amplitude profile as a function of a given bifurcation parameter usually presents a discontinuity between these two regimes, which makes the NES potentially very sensitive to uncertainties. In Snoun et al. (2020), this discontinuity is predicted by means of a ME-gPC based method. This allows to determine the Propensity of the system to undergo a Harmless Steady-State Regime (PHSSR), which is defined as the probability for the system to undergo a mitigated regime. The aim of this paper is therefore to maximize the PHSSR value to obtain a robust optimal design of the NES with a low computational cost. For this purpose, several stochastic optimization problems are presented for a PS having uncertain parameters, in which the NES parameters are either considered as deterministic, or are also supposed uncertain but with a known probability law.

The article is organized as follows. In Section 2, the two degrees-of-freedom Hultèn's model coupled to two NES is presented. In Section 3, the possible steady-state regimes of the coupled system are studied, and the PHSSR is defined. Section 4 describes the polynomial chaos theory and recalls the stochastic optimization algorithm used to compute the PHSSR. The optimization formulation under uncertainties is described in Section 5, and the results are presented in Section 6. Finally, conclusions are given in Section 8.

2. The friction system under study

The studied mechanical system is similar to that previously used by the authors in Bergeot et al. (2017); Snoun et al. (2020). It is recalled hereafter for the sake of clarity.

2.1. The primary system

The primary system (PS) consists in the two degree-of-freedom (DOF) Hultèn's phenomenological model (Hultén (1997, 1993)). This simple model can reproduce the mode-coupling phenomenon and is composed of a mass m held against a moving strip. The contact between the mass and the strip is modeled by two plates supported by two different springs, with linear components k_1 and k_2 and cubic components k_1^{NL} and k_2^{NL}, and two dampers with damping coefficients c_1 and c_2 (see Fig. 1). We assume that the friction coefficient is constant and that the strip moves at a constant velocity. The relative velocity between the strip velocity and dx_1/dt or dx_2/dt is supposed to be positive,

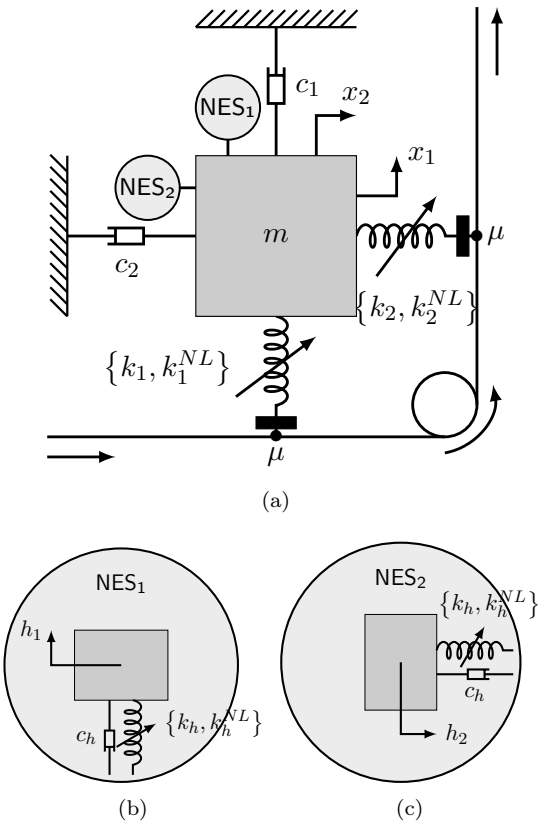

Figure 1: The mechanical model. (a) Mechanical system with NES; (b) Zoom on NES_1; (c) Zoom on NES_2.

and the friction contact is modeled by the Coulomb's law, i.e. $F_T = \mu F_N$ where F_T is the tangential friction force, F_N is the normal force and μ is the friction coefficient. Using Newton's second law the equations of motion, that constitute the primary system in this work, are derived as follows:

$$m\ddot{x}_1 + c_1\dot{x}_1 + k_1x_1 - \mu k_2x_2 + k_1^{NL}x_1^3 - \mu k_2^{NL}x_2^3 = 0 \quad (1a)$$

$$m\ddot{x}_2 + c_2\dot{x}_2 + k_2x_2 + \mu k_1x_1 + \mu k_1^{NL}x_1^3 + k_2^{NL}x_2^3 = 0. \quad (1b)$$

2.2. Mechanical model with Nonlinear Energy Sinks

Two strongly cubic and identical ungrounded NES with masses m_h, damping coefficients c_h and cubic stiffnesses k_h^{NL}, are attached on the primary system (see Fig. 1). Introducing the NES displacements $h_1(t)$ and $h_2(t)$ in Eq. (1) leads to the following equations of motion of the coupled system

$$\ddot{x}_1 + \eta_1\omega_1\dot{x}_1 + \omega_1^2x_1 - \mu\omega_2^2x_2 + \varphi_1x_1^3 - \mu\varphi_2x_2^3 + \eta_h\omega_1\left(\dot{x}_1 - \dot{h}_1\right) + \xi_h\left(x_1 - h_1\right) + \varphi_h\left(x_1 - h_1\right)^3 = 0 \quad (2a)$$

$$\epsilon\ddot{h}_1 + \eta_h\omega_1\left(\dot{h}_1 - \dot{x}_1\right) + \xi_h\left(h_1 - x_1\right) + \varphi_h\left(h_1 - x_1\right)^3 = 0 \quad (2b)$$

$$\ddot{x}_2 + \eta_2\omega_2\dot{x}_2 + \omega_2^2x_2 + \mu\omega_1^2x_1 + \mu\varphi_1x_1^3 + \varphi_2x_2^3 + \eta_h\omega_1\left(\dot{x}_2 - \dot{h}_2\right) + \xi_h\left(x_2 - h_2\right) + \varphi_h\left(x_2 - h_2\right)^3 = 0 \quad (2c)$$

$$\epsilon\ddot{h}_2 + \eta_h\omega_1\left(\dot{h}_2 - \dot{x}_2\right) + \xi_h\left(h_2 - x_2\right) + \varphi_h\left(h_2 - x_2\right)^3 = 0, \quad (2d)$$

where $\eta_i = c_i/\sqrt{mk_i}$ (with $i = 1, 2$) are the relative damping coefficients, $\omega_i = \sqrt{k_i/m}$ are the natural angular frequencies, $\varphi_i = k_i^{NL}/m$; as for the NES parameters, $\epsilon = m_h/m$ is the mass ratio between the NES and the primary structure, $\xi_h = k_h/m$, $\eta_h = c_h/\sqrt{mk_1}$ and $\varphi_h = k_h^{NL}/m$. Because strongly cubic NES are considered, one has $\xi_h \ll \varphi_h$. In general, the mass ratio ϵ is in the range $0.01 - 0.1$ as in the present paper.

3. Possible steady-state regimes

Four main types of steady-state regimes (SSR) may be generated when one or several NES are attached on a primary system which undergoes an LCO: complete suppression of the instability, mitigation through Periodic Response (PR), mitigation through Strongly Modulated Response (SMR) or no mitigation. Those four regimes can also be observed on the studied system (2) (Bergeot et al. (2017)), and are presented in Fig. 2 which shows for each case the displacements $x_1(t)$ - with and without NES attachments - with respect to time. The regimes described above are classified into two categories depending on whether the LCO is considered as mitigated (Figs. 2(a), 2(b) and 2(c)) or not (Fig. 2(d)).

In this work the Quantity of Interest (QoI) under consideration is the amplitude $A_{x_1}^{wNES}$ of the variable x_1 in the system with NES (2) and within a steady-state regime. It is defined as follows

$$A_1^{\text{wNES}} = \frac{\max\left[x_1^{SSR}(t)\right] - \min\left[x_1^{SSR}(t)\right]}{2}, \quad (3)$$

where $x_1^{SSR}(t)$ is the times series of the variables x_1 obtained from the numerical integration of the coupled system (2) within the steady-state regime. For comparison purposes, the amplitude A_1^{woNES} of the system without NES (1) is also computed.

The time integration of system (2) (resp. (1)) is performed between $t_b = 0$ and $t_e = 4$ seconds and the amplitude A_1^{wNES} (resp. A_1^{woNES}) is computed in the interval $[0.9t_e\ t_e]$ in which we assume that the system has reached its steady-state regime.

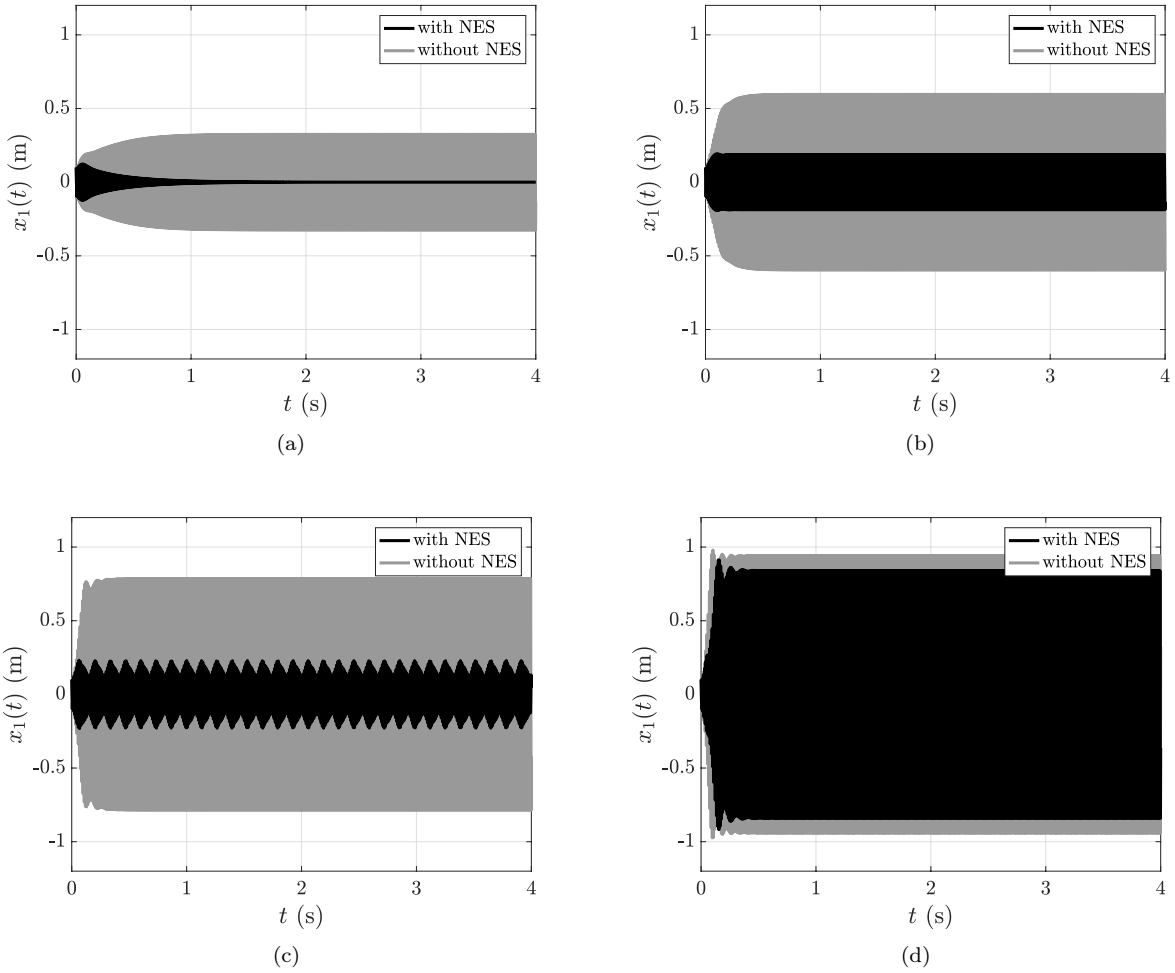

Figure 2: Comparison between time series $x_1(t)$ resulting from the numerical integration of the friction system with and without NES. (a) Complete suppression, $\mu = 0.16$; (b) Mitigation: PR, $\mu = 0.18$; (c) Mitigation: SMR, $\mu = 0.2$; (d) No mitigation, $\mu = 0.22$. The set of parameters Eq. (4) has been used.

Using the following set of parameters

$$\begin{aligned} &\omega_1 = 2\pi 100 \ (\text{rad}\cdot\text{s}^{-1}), \quad \omega_2 = 2\pi 85 \ (\text{rad}\cdot\text{s}^{-1}), \\ &\eta_1 = 0.02, \quad \eta_2 = 0.06, \\ &\varphi_1 = 10^5 \ (\text{N}\cdot\text{kg}^{-1}\cdot\text{m}^{-3}), \quad \varphi_2 = 0 \ (\text{N}\cdot\text{kg}^{-1}\cdot\text{m}^{-3}), \\ &\epsilon = 0.05, \quad \xi_h = 0.001 \ (\text{N}\cdot\text{kg}^{-1}\cdot\text{m}^{-1}), \\ &\eta_h = 0.02, \quad \varphi_h = 1.4\cdot 10^5 \ (\text{N}\cdot\text{kg}^{-1}\cdot\text{m}^{-3}), \end{aligned} \tag{4}$$

the amplitudes A_1^{wNES} and A_1^{woNES} are plotted as functions of the friction coefficient μ in Fig. 3. The specific values of μ denoted as $\mu_{\text{b}}^{\text{wo}}$ and $\mu_{\text{b}}^{\text{w}}$ correspond to the Hopf bifurcation points without and with the NES attachments, respectively. The four steady-state regimes described above are visible on the Figure, which highlights a discontinuity (or jump) in the profile of A_1^{wNES}. For increasing values of μ, this discontinuity corresponds in general to the transition from the SMR to the no suppression regime and separates mitigated regimes from unmitigated ones. The value of μ at the discontinuity is called mitigation limit

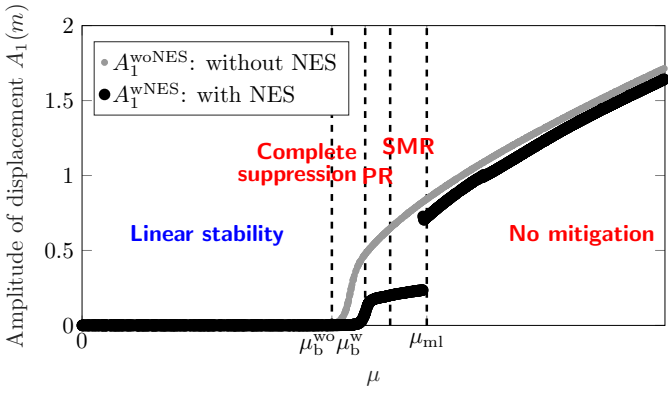

Figure 3: Amplitudes A_1^{wNES} and A_1^{woNES} as functions of the friction coefficient μ. The set of parameters Eq. (4) has been used.

and is denoted as μ_{ml}.

The Propensity to be in a Harmless Steady-State Regime

(PHSSR) (Snoun et al. (2020)) can be computed from the mitigation limit μ_{ml}. The PHSSR is the probability of obtaining a mitigated regime given the probability laws governing the dispersion of the primary system parameters. Here, only μ is considered as uncertain and it is assumed to follow a uniform probability law within the interval $[0, \mu_e = 0.4]$; the PHSSR is then simply defined as

$$\text{PHSSR} = \int_0^{\mu_{\text{ml}}} \frac{1}{\mu_e} d\mu = \frac{\mu_{\text{ml}}}{\mu_e}. \tag{5}$$

4. Multi-Element Polynomial Chaos based algorithm to detect a discontinuity

The ME-gPC method previously developed by the authors in Snoun et al. (2020) to locate the discontinuity in the QoI profile is recalled in Section 4.2. Elements of the Polynomial Chaos theory are first presented in Section 4.1.

4.1. Elements of the Polynomial Chaos theory

4.1.1. Generalized Polynomial Chaos (gPC)

Let us consider a dynamical system with r uncertain physical parameters β_j $(j = 1, \ldots, r)$ assumed to be uniformly distributed within a given space $\prod_{i=1}^{r}[a_i, b_i]$, and let ξ_j $(j = 1, \ldots, r)$ be the independent random variables within the space $[-1\ 1]^r$, linked to β_j by

$$\beta_j(\xi_j) = \frac{a_j + b_j}{2} + \frac{b_j - a_j}{2}\xi_j, \quad (j = 1, \ldots, r). \tag{6}$$

The gPC theory (Wiener (1938); Cameron and Martin (1947); Xiu and Karniadakis (2002)) states that the system output variable $X(\xi_1, ..., \xi_r)$, called the quantity of Interest (QoI), may be approximated by a truncated orthogonal polynomial function series as

$$X(\xi_1, ..., \xi_r) \approx \sum_{j=0}^{N_p} \bar{x}_j \phi_j(\xi_1, ..., \xi_r), \tag{7}$$

where $\phi_j(\xi)$ are orthogonal polynomials which represent the stochastic part of the process, whereas $\bar{x}_j$ are the gPC coefficients that take into account the deterministic part of the process. In this paper, according to the Askey-scheme (Askey and Wilson (1985)), the orthogonal polynomials $\phi_j(\xi_1, ..., \xi_r)$ are built from Legendre polynomials because the uncertain parameters follow a uniform probabilistic law. From Xiu and Karniadakis (2002), the number of terms $N_p + 1$ of the expansion is given by

$$N_p + 1 = \frac{(p + r)!}{p!r!}, \tag{8}$$

where r is the number of uncertain parameters and p is the order of the gPC. To obtain the approximated values of the QoI X, the coefficients $\bar{x}_j$ of the truncated series (7) must be computed. To that end, the non-intrusive regression method (Berveiller et al. (2006)) is used in this paper. In this method, the gPC coefficients are built from Q values of the QoI X. The corresponding Q simulations may be performed at points chosen with the Latin Hypercube Samples (LHS) method (McKay et al. (1979)) that will be referred to as the Numerical Experimental Design (NED) in this paper. A minimum of $Q = N_p$ simulations is required but in practice, $Q = kN_p$ simulations are used, with k a small integer usually equal to 2, 3 or 4.

4.1.2. Multi-Element Generalized Polynomial Chaos (ME-gPC)

When the QoI is nonlinear, high polynomial orders may be required to reduce the approximation error. Thus, when the number of uncertain parameters r is high, the number of simulations required to compute the gPC coefficients may be excessive, leading to a prohibitive computational cost. An alternative is to split the vector $\xi = (\xi_1, ..., \xi_r)$ into a collection of m non-intersecting elements and to use a low order polynomial approximation on each element. That is the basic idea behind the ME-gPC Wan and Karniadakis (2005).

The local physical variables β_j^k, in the k^{th} element $\prod_{i=1}^{r}[a_i^k, b_i^k]$, are expressed in terms of independent uniform random variables ξ_j^k in $[-1, 1]^r$ through

$$\beta_j^k = \frac{b_j^k + a_j^k}{2} + \frac{b_j^k - a_j^k}{2}\xi_j^k. \tag{9}$$

Consequently, Legendre polynomials can be used locally and a gPC expansion developped in each element as follows:

$$X_k(\bar{\xi}^k) \approx \sum_{j=0}^{N_p} \bar{x}_{k,j} \phi_j(\bar{\xi}^k), \tag{10}$$

where $X_k(\bar{\xi}^k)$ is the random process corresponding to the k^{th} element.

From the gPC theory, the approximated local mean $\hat{X}_{p,k}$ and variance $\sigma_{p,k}^2$ in the k^{th} element can be expressed analytically from the gPC coefficients as

$$\begin{cases} \hat{X}_{p,k} = \bar{x}_{k,0} \\ \sigma_{p,k}^2 = \dfrac{1}{2^r} \displaystyle\sum_{j=1}^{N_p} \bar{x}_{k,j}^2 \langle \phi_j^2 \rangle. \end{cases} \tag{11}$$

Several criteria have been proposed in the literature for the convergence of the ME-gPC algorithm. They depend on the aim of the ME-gPC. The criteria chosen in this study are presented in the next section.

4.2. Detection of a discontinuity in the QoI with the ME-gPC

This section recalls the method based on the ME-gPC and proposed in Snoun et al. (2020) to locate a discontinuity in a Quantity of Interest (QoI) derived from the DM of a mechanical system. The aim of the method is not necessarily to obtain an accurate representation of the QoI, but to locate precisely the discontinuity, i.e. to know the values

of the uncertain parameters for which the discontinuity in the QoI profile appears.

The underlying principle of the method is that the variance of a QoI that contains a discontinuity is higher than that of a QoI that does not contain any discontinuity. Therefore, if the discontinuity lies in a given element of the stochastic parameter space, the variance of the ME-gPC expansion in that element will be high. From these considerations a ME-gPC algorithm has been built, in which at each step and for each element the local variance $\sigma^2_{p,k}$, computed directly from the gPC coefficients using Eq. (11), is compared to a threshold θ_1. If for a given element k

$$\sigma^2_{p,k} \geq \theta_1, \tag{12}$$

it is assumed that the discontinuity lies within this element. The latter is then divided by two in each direction of the stochastic space in order to locate more accurately the discontinuity. On the contrary, if the condition Eq. (12) is not satisfied, the element k is supposed not to contain the discontinuity and is removed from the algorithm.

The threshold θ_1 is chosen so that the variance of the element which contains the discontinuity always satisfies the condition Eq. (12). Therefore, two other criteria are introduced to stop the algorithm. The first one is the minimum element size $J_{\min}$ defined as

$$J_{\min} = \theta_2 J_0, \tag{13}$$

where J_0 is the size of the initial element corresponding to the whole stochastic parameter space and θ_2 is a percentage. At a given iteration i, the retained elements of size J_i are actually divided into two equal parts in each direction of the stochastic space if the following condition

$$J_i \geq J_{\min} \tag{14}$$

holds. It is worth recalling that all the elements at iteration i have the same size J_i because at each step the division is performed in each direction of the stochastic. If the condition (14) does not hold, the algorithm is stopped and we assume that the discontinuity in the QoI profile lies within the remaining elements.

In Section 6, a comparison is performed with a reference method that needs N simulations of the DM to locate a discontinuity in the QoI profile. Therefore, the proposed method is only effective if the number of numerical simulations N' required to obtain the gPC coefficients in all the elements is smaller than N. Consequently, the second criterion is that N' should verify

$$N' \leq N, \tag{15}$$

otherwise the algorithm is stopped.

The algorithm is summarized in Fig. 4. At the first step, only one element is present (i.e. the whole stochastic parameter space) and for a given iteration the parameter space has been divided into K elements during the previous iterations. At each iteration, the gPC coefficients are

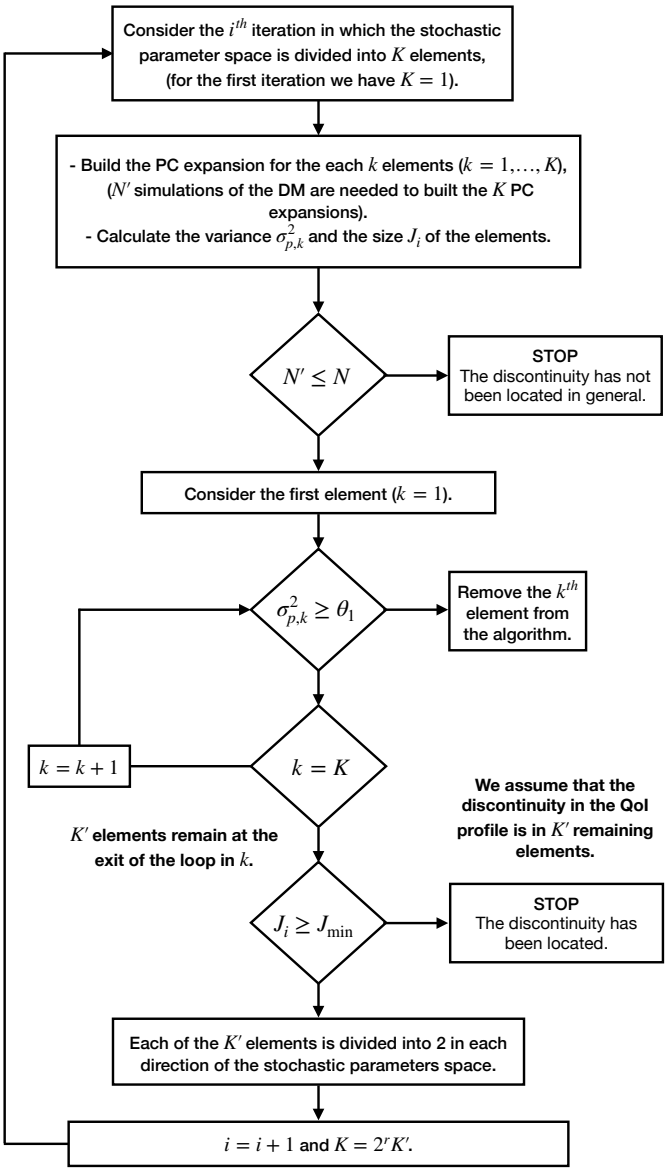

Figure 4: Algorithm of the proposed method based on the ME-gPC.

computed for the K elements and we check if the corresponding computational cost is larger than the reference one (see Eq. (15)). If that is the case, the algorithm is stopped and in general the discontinuity in the QoI profile has not been located. If Eq. (15) holds, we check the variance in each of the K elements (see Eq. (13)). If it is smaller than the threshold θ_1, the element is removed from the algorithm. If it is larger, it is kept and K' elements remain at the exit of the loop in k. If Eq. (14) does not hold, the algorithm is stopped and we assume that the discontinuity in the QoI profile lies within the K' remaining elements. If Eq. (14) holds, then each of the K' elements is divided into two parts in each direction of the stochastic parameter space, then a new iteration begins with $K = 2^r K'$.

As for the reference method, the detection of the discontinuity can be performed by the so-called Jump Criterion (JC). To be considered as an effective jump, the difference between the amplitude at the right of the jump, denoted as $A(\mu_{\text{ml}}^{+})$, and the amplitude at the left, denoted as $A(\mu_{\text{ml}}^{-})$, must be greater than the half of $A(\mu_{\text{ml}}^{-})$, i.e.

$$\text{JC} = \frac{A(\mu_{\text{ml}}^{+}) - A(\mu_{\text{ml}}^{-})}{A(\mu_{\text{ml}}^{-})} \geqslant \frac{1}{2}. \tag{16}$$

As an example, Fig. 5 shows the last iteration of the algorithm applied to the system (2) for $\theta_1 = 0.7{\cdot}10^{-3}$, $\theta_2 = 1\%$ and $p = 1$. The Reference curve is similar to that displayed in Fig. 3. One can see that the last interval obtained with the ME-gPC method contains the discontinuity observed on the reference.

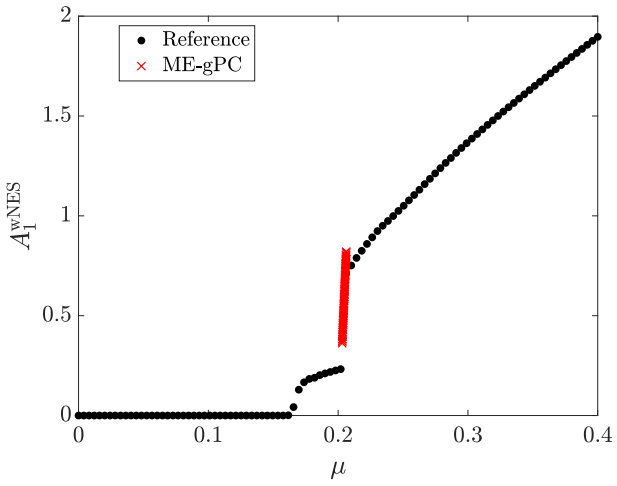

Figure 5: Last iteration of the detection algorithm when the friction coefficient μ is uncertain, with $\theta_1 = 0.7 \cdot 10^{-3}$, $\theta_2 = 1\%$ and $p = 1$; reference curve obtained from Fig. 3.

5. Optimization strategy under uncertainties

This section focuses on the optimization methodology proposed to maximize the PHSSR defined in Section 3. Two NES parameters are retained as the design parameters to optimize: the damping coefficient η_h and the nonlinear stiffness φ_h. The uncertain parameter is again the friction coefficient μ. Following Boroson et al. (2017); Pidaparthi and Missoum (2019), the problem is treated in two different ways depending on whether the physical design parameters η_h and φ_h are deterministic or stochastic.

5.1. Deterministic design variables

In this case, the parameters to optimize are directly the physical design parameters which are assumed to be known with certainty. The objective of the method is to find the optimal values of the NES parameters x_d that maximize the PHSSR value. For this purpose, the PHSSR is determined in the space of uncertain parameters x_u for each value of $x_d \in [x_d^{(\min)}\ x_d^{(\max)}]$. The maximum of the PHSSR is then detected, which corresponds to the optimal value of x_d. The method can be summarized as follows:

$$\begin{aligned} &\text{Maximize} && \text{PHSSR } (A(x_d, x_u)) \\ &\text{Subject to} && x_d^{(\min)} \leqslant x_d \leqslant x_d^{(\max)} \\ &\text{where} && x_d = \{\eta_h, \varphi_h\}, \\ & && x_u = \{\mu\} \end{aligned} \tag{17}$$

where

- $A(x_d, x_u)$ is the amplitude of the displacement of the coupled system (2) defined by Eq. (3) (from now on the amplitude is simply written A instead of A_1^{wNES} to lighten the notations); it depends on both the uncertain parameters x_u and the design variables x_d;
- $x_d^{(\min)}$ and $x_d^{(\max)}$ are the minimum and maximum values of the design variables x_d respectively; the optimal values of the design parameters are searched within the intervals $[x_d^{(\min)}\ x_d^{(\max)}]$, called *design intervals*.

5.2. Stochastic design variables

The physical design parameters are considered here to be random with a known probability law. This case is closer to a real situation, as it is known in particular that obtaining an exact value of a damping coefficient is almost impossible. The parameters to be optimized are then statistical characteristics of these physical parameters (for instance their means or variances) and are called *hyperparameters*. In this study the hyperparameters considered are the means $\hat{\eta}_h$ and $\hat{\varphi}_h$ of the damping coefficient and of the cubic stiffness of the NES, respectively.

The optimization process consists in dividing the design space into subspaces. In each subspace a draw of N values of the design parameters is performed according to their probability laws (in this work we use uniform laws). For each of these N values the PHSSR is calculated and the optimal value of x_d (here of $\hat{\eta}_h$ or $\hat{\varphi}_h$) corresponds to the subspace where the mean of the N PHSSR values is maximum. This can be summarized as follows:

$$\begin{aligned} &\text{Maximize} && \mathbf{E}[\text{PHSSR } (A(x_d, x_u))] \\ &\text{Subject to} && x_d^{(\min)} \leqslant x_d \leqslant x_d^{(\max)} \\ &\text{where} && x_d = \{\hat{\eta}_h, \hat{\varphi}_h\}, \\ & && x_u = \{\mu\} \end{aligned} \tag{18}$$

where

- $\mathbf{E}$ is the value of the mathematical expectation (the mean) of all PHSSR evaluations;
- $\hat{\eta}_h$ is the mean of the NES damping coefficient values;
- $\hat{\varphi}_h$ is the mean of the NES cubic stiffness values.

6. Results for deterministic design variables

As explained before, the first method of NES optimization considers that the NES parameters are deterministic and constitute therefore directly the design variables to optimize.

6.1. Optimization of the NES damping coefficient

In this section, we consider first that the design space is a one-dimensional space according to the variable η_h, represented by the interval $[0, 0.04]$. The optimization problem (17) is therefore solved with $x_d = \eta_h \in [0, 0.04]$ with the other parameters given Eq. (4). The results are expressed in terms of computational cost, on the one hand, and of precision compared to the reference method, on the other hand. For this purpose, the following quantities are introduced:

- $\mu_{\text{ml}}^{\max}$ is the maximum value of the mitigation limit μ_{ml}, and corresponds to the maximum value of the PHSSR, denoted as $\text{PHSSR}^{\max}$. The mitigation limit is here searched within the interval $[0, 0.4]$. The PHSSR value estimated by the ME-gPC method is determined using the upper bounds of the last intervals found by the algorithm presented in Fig. 5. The precision of the corresponding $\mu_{\text{ml}}^{\max}$ value is therefore given by:
$$\mu_{\text{ml}}^{\max} \pm \frac{\Delta\mu}{\mu_{\text{ml}}^{\max}}. \tag{19}$$
For the reference method, $\Delta\mu$ is given by the discretization step of the design space, whereas $\Delta\mu = 0.4\theta_2$, whith θ_2 defined by Eq. (13), for the ME-gPC method.

- $E_{\text{PHSSR}^{\max}}$ is the relative error of the maximum PHSSR obtained with the ME-gPC method ($\text{PHSSR}_{\text{ME-gPC}}^{\max}$) compared to the maximum PHSSR value obtained with the reference method ($\text{PHSSR}_{\text{ref}}^{\max}$), and is defined as follows:
$$E_{\text{PHSSR}^{\max}} = \frac{\left|\text{PHSSR}_{\text{ME-gPC}}^{\max} - \text{PHSSR}_{\text{ref}}^{\max}\right|}{\text{PHSSR}_{\text{ref}}^{\max}}. \tag{20}$$

- η_h^{opt} is the optimal value of the NES damping coefficient, i.e. the value for which $\mu_{\text{ml}}^{\max}$, and thus $\text{PHSSR}^{\max}$, are obtained. Since the design space is discretized with a step $\Delta\eta_h$, the optimal value is expressed as follows
$$\eta_h^{\text{opt}} \pm \frac{\Delta\eta_h}{\eta_h^{\text{opt}}}. \tag{21}$$

- Err is the relative error of the optimal design value η_h^{opt} obtained with the ME-gPC method, compared to that obtained with the reference method:
$$Err = \frac{\left|(\eta_h^{\text{opt}})_{\text{ME-gPC}} - (\eta_h^{\text{opt}})_{\text{ref}}\right|}{(\eta_h^{\text{opt}})_{\text{ref}}}. \tag{22}$$

6.1.1. Reference optimization

The reference value of the optimal NES damping coefficient, denoted as $(\eta_h^{\text{opt}})_{\text{ref}}$, is obtained by solving (17) where the amplitude $A(x_d, x_u)$, and thus the mitigation limit, directly result from the numerical simulation of (2). The design space for η_h $[0, 0.04]$ is uniformly discretized into 51 values. To reduce the computational cost, the mitigation limit μ_{ml} and the PHSSR are first roughly estimated for each η_h value using only 1000 values of the friction coefficient $\mu \in [0, 0.4]$ and applying the criterion (16). Fig. 6 shows the resulting evolution of the PHSSR as a function of η_h. This first step enables the locating of the interval - here $[0.0208, 0.028]$ - in which the optimal value of the design parameter $(\eta_h^{\text{opt}})_{\text{ref}}$ lies. In this interval the PHSSR is maximum ($\text{PHSSR}^{\max} = 50.10\% \pm 0.19\%$) but constant due to the too coarse discretization in μ. To refine this reference result, the PHSSR is then calculated in the design interval $\eta_h \in [0.02, 0.03]$ with the same discretization step for η_h as previously, but now with 10 000 values of μ to determine the mitigation limit for each value of η_h. The total number of simulations needed to obtain the reference value is therefore equal to $50 \times 1000 + 10 \times 10\,000 = 150\,000$.

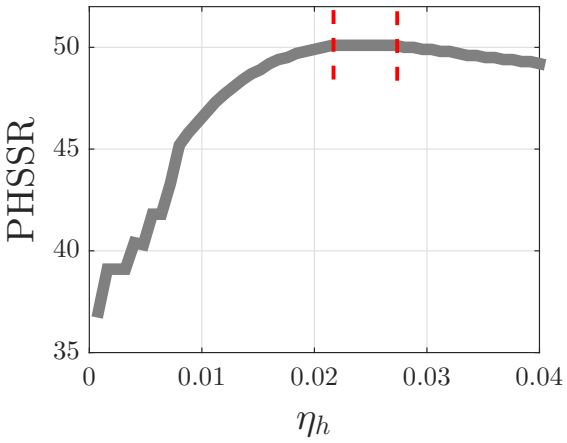

Figure 6: Result of the first step of the reference optimization procedure: PHSSR as a function of η_h, for $\varphi_h = 140\,000$ N·kg^{-1}·m^{-3}.

Fig. 7 shows the new PHSSR as a function of η_h. In this case, $(\mu_{\text{ml}}^{\max})_{\text{ref}} = 0.2004 \pm 0.02\%$ which gives $(\text{PHSSR}^{\max})_{\text{ref}} = 50.1\% \pm 0.02\%$. The corresponding optimal design value of the damping coefficient is $(\eta_h^{\text{opt}})_{\text{ref}} = 0.0240 \pm 3.33\%$.

6.1.2. Optimization with the ME-gPC method

In the proposed approach, the optimal value of the NES damping coefficient, denoted as $(\eta_h^{\text{opt}})_{\text{ME-gPC}}$, is still obtained by solving (17), but the amplitude $A(x_d, x_u)$ and the mitigation limit (17) are now determined by the method based on the ME-gPC.

Three optimization procedures are applied with a gPC order $p = 1$, a variance threshold $\theta_1 = 2 \cdot 10^{-3}$ and three values of the element size threshold: $\theta_2 = 1\%$, 0.1% and

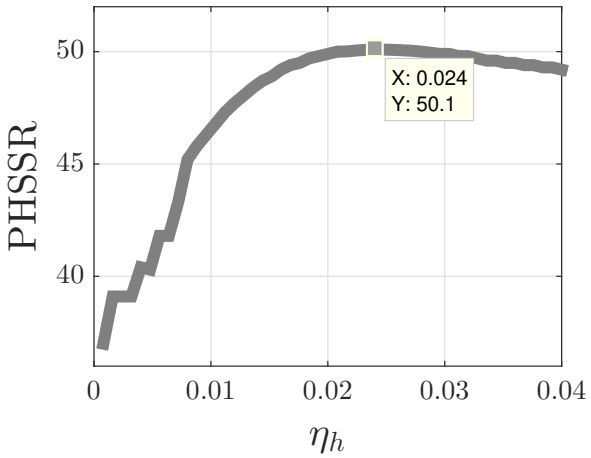

Figure 7: Result of the second step of Reference optimization: PHSSR as a function of η_h, for $\varphi_h = 140\,000$ N·kg^{-1}·m^{-3}.

0.001%. The results of this ME-gPC based optimization are presented in Tab. 1, along with the reference results for comparison.

Fig. 8 displays the variations of the PHSSR as functions of η_h respectively obtained with the reference method and the three ME-gPC methods with $\theta_2 = 1\%$, 0.1% and 0.001%. For $\theta_2 = 1\%$ the number of simulations is equal to 4324, the optimal value is $(\eta_h^{\text{opt}})_{\text{ME-gPC}} = 0.0241 \pm 15.14\%$ and the maximum value of the corresponding PHSSR is 50.78%, implying an error compared to the reference solution $E_{\text{PHSSR}^{\max}} = 1.35\%$. In the case of $\theta_2 = 0.1\%$, although the new value of θ_2 has no influence on η_h^{opt}, it changes the maximum value of the PHSSR to $\text{PHSSR}^{\max}_{\text{ME-gPC}} = 50.09\%$ which induces a relative error $E_{\text{PHSSR}^{\max}} = 0.02\%$. This error is lower than the previous one (with $\theta_2 = 1\%$) but the number of simulations has increased and is now equal to 5165. For $\theta_2 = 0.001\%$ the optimal value becomes $(\eta_h^{\text{opt}})_{\text{ME-gPC}} = 0.0237 \pm 3.33\%$, implying a relative error $Err = 1.25\%$ compared to the reference value, which is higher than the errors in the previous cases. This is not illogical since the error is calculated according to the midpoints of the intervals. Nevertheless, the interval obtained with $\theta_2 = 0.001\%$ is much narrower ($\pm 3.33\%$) than that obtained with $\theta_2 = 0.01\%$ ($\pm 15.14\%$), and contains the value resulting from the reference method. The total number of simulations is in this last case equal to 7026, which remains 22 times smaller than the number needed with the reference method.

The plateaus observed in Fig. 8 are due to the fact that for two close values of η_h the mitigation limits are found in the same element. They are related to the value of the threshold θ_2: the lower it is, the more accurate the localization of the mitigation limit is, with in counterpart an increase of the computational cost. The precision is therefore driven by the value of the threshold θ_2.

Finally, with a computational cost much lower than the reference one, the proposed approach proves efficient to identify the value of the optimal NES damping coefficient while taking into account the dispersion of the friction coefficient.

6.2. Optimization of the NES nonlinear stiffness

The aim of this section is to find the optimal value of the cubic stiffness of the NES φ_h assumed here to be deterministic. The damping coefficient value η_h is here set to 0.024. Similarly to the previous section, the following quantities are defined:

- φ_h^{opt} is the optimal value of the NES cubic stiffness for which $\mu_{\text{ml}}^{\max}$, and thus $\text{PHSSR}^{\max}$, are obtained. It may be again expressed with respect to the discretization step $\Delta\varphi_h$ of the design space as

$$\varphi_h^{\text{opt}} \pm \frac{\Delta\varphi_h}{\varphi_h^{\text{opt}}}. \tag{23}$$

- Err is now the relative error of the optimal design value φ_h^{opt} obtained with the ME-gPC method, compared to that obtained with the reference method:

$$Err = \frac{|(\varphi_h^{\text{opt}})_{\text{ME-gPC}} - (\varphi_h^{\text{opt}})_{\text{ref}}|}{(\varphi_h^{\text{mid}})_{\text{ref}}}. \tag{24}$$

6.2.1. Reference optimization

The same strategy has been applied for the reference optimization of the NES cubic stiffness φ_h. First, to get an idea of the shape of the PHSSR as a function of φ_h, a small number of simulations is performed with a discretization step equal to 10 on the design space $\varphi_h \in [0, 900\,000]$ N·kg^{-1}·m^{-3}. For each value of φ_h the PHSSR is computed using 1000 values of μ within the interval $[0, 0.4]$. Fig. 9 shows the resulting evolution of the PHSSR as a function of φ_h. The mitigation limit appears to decrease monotonically with the cubic stiffness value. The optimal value φ_h^{opt} is therefore the lowest value of φ_h for which the jump criterion (16) is met and is found equal to 100 000 N·kg^{-1}m^{-3}.

The next step then consists in focusing on a reduced design space composed of the lowest values of φ_h in order to understand the dynamic behavior of the system for these values and to refine the optimization result. The retained design interval $\varphi_h \in [0, 150\,000]$ N·kg^{-1}·m^{-3} is uniformly discretized into 100 values, and for each one the mitigation limit is directly computed from (2) using again 1000 values of μ within $[0, 0.4]$ interval. The number of simulations is thus equal to $100 \times 1000 = 100\,000$.

Fig. 10 shows the evolutions of the jump criterion (16) and of the PHSSR as functions of φ_h, respectively. For low values of φ_h ($\varphi_h \in [0\ 46\,970]$ N·kg^{-1}·m^{-3} a jump exists but, as mentioned before, we consider that the difference between the amplitudes of the limit cycles before and after the jump is too small for the concerned regimes to be qualified as mitigated. The difficulty of this optimization problem is then to find the lowest value

Table 1: Comparison between the reference optimization and the ME-gPC optimization considering deterministic design variables. The design parameter is η_h. The reference results are obtained as described in Sect. 6.1.1.

	Nb of simulations	Computational time	$\text{PHSSR}^{\max}$	$E_{\text{PHSSR}^{\max}}$	η_h^{opt}	Err
Reference	150 000	2.15 days	$50.10\% \pm 0.02\%$	–	$0.0240 \pm 3.33\%$	–
ME-gPC ($\theta_1 = 2 \cdot 10^{-3}$ and $\theta_2 = 1\%$)	4324	1.70 hours	$50.78\% \pm 1.97\%$	1.35%	$0.0241 \pm 15.14\%$	0.41%
ME-gPC ($\theta_1 = 2 \cdot 10^{-3}$ and $\theta_2 = 0.1\%$)	5165	2.06 hours	$50.09\% \pm 0.2\%$	0.02%	$0.0241 \pm 15.14\%$	0.41%
ME-gPC ($\theta_1 = 2 \cdot 10^{-3}$ and $\theta_2 = 0.001\%$)	7026	3.23 hours	$50.09\% \pm 0.02\%$	0.02%	$0.0237 \pm 3.33\%$	1.25%

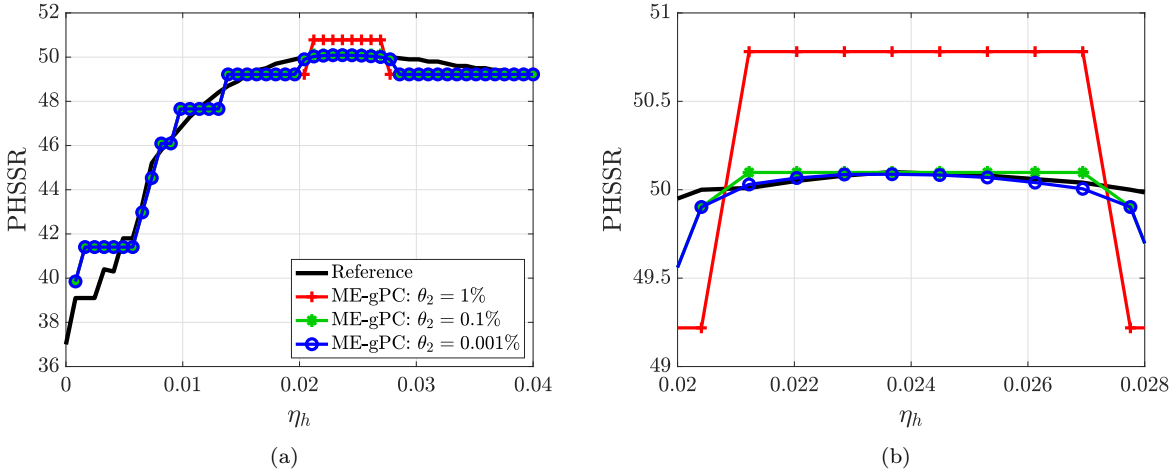

Figure 8: Comparison between the optimization strategies based on the reference method and the ME-gPC for $\eta_h \in [0\ 0.04]$ with $\varphi_h = 140\,000$ $\text{N}\cdot\text{kg}^{-1}\cdot\text{m}^{-3}$. (a) PHSSR and (b) Zoom of the PHSSR. The reference results are obtained as described in Sect. 6.1.1.

of φ_h for which the discontinuity jump is high enough. It is clear that the solution depends on the value of the threshold for the jump criterion (here 50%). The optimal value here is therefore $(\varphi_h^{\text{opt}})_{\text{ref}} = 46\,970 \pm 3.22\%$ $\text{N}\cdot\text{kg}^{-1}\cdot\text{m}^{-3}$, which corresponds to the maximum PHSSR value $\text{PHSSR}^{\max} = 52.25\% \pm 0.19\%$. The PHSSR curve exhibits again stationary phases linked to the discretization step for μ. Indeed, for two close values of φ_h, the discontinuities in the amplitude profiles as functions of μ appear for very close μ values whose difference is smaller than the discretization step.

6.2.2. Optimization with the ME-gPC method

We denote by $(\varphi_h^{\text{opt}})_{\text{ME-gPC}}$ the optimal value of the NES cubic stiffness coefficient obtained by solving (17) where the amplitude $A(x_d, x_u)$ and the mitigation limit are assessed using the ME-gPC based method.

The gPC order is again set to $p = 1$ and the mitigation limit, as explained before, is approached by the upper bound of the last element found. Tab. 2 compares the results obtained with this ME-gPC method, for several thresholds values θ_1 and θ_2, to those arising from the reference procedure (in which, as detailed in the previous section, the values of φ_h are taken from the design space $[0, 150\,000]$ $\text{N}\cdot\text{kg}^{-1}\cdot\text{m}^{-3}$ which is uniformly discretized).

Fig. 11 shows the evolution of the PHSSR as a function of φ_h for $\theta_1 = 3.5 \cdot 10^{-3}\%$ and $\theta_2 = 0.1\%$.

For a given value of the threshold θ_2, it can be observed from Tab. 2 that the precision of the results depends on the jump threshold θ_1. Indeed, when the value of θ_1 increases, the error $\text{PHSSR}^{\max}$ decreases from 3.15% to 1.68% and the error Err decreases from 29.03% to 3.22%. Another benefit of increasing θ_1 is that it reduces the number of required simulations, as can be seen in Tab. 2. However, for higher values of θ_1, the ME-gPC method appears unable to detect the discontinuity in the amplitude profile, as the jump in the amplitude values becomes lower than the threshold θ_1, which makes the research of the opti-

Table 2: Comparison between the reference optimization and the Me-gPC based optimization considering deterministic design variables. The design parameter is φ_h. The reference results are obtained as described in Sect. 6.2.2.

	Nb of simulations	Computational time	$\text{PHSSR}^{\max}$	$E_{\text{PHSSR}^{\max}}$	φ_h^{opt}	Err
Reference	100 000	1.49 days	52.25% ± 0.19%	–	46 970 ± 3.22%	–
ME-gPC ($\theta_1 = 3.3 \cdot 10^{-3}$ and $\theta_2 = 1\%$)	6 652	2.64 hours	53.90% ± 1.86%	3.15%	33 333 ± 4.50%	29.03%
ME-gPC ($\theta_1 = 4.2 \cdot 10^{-3}$ and $\theta_2 = 1\%$)	5 817	2.31 hours	53.13% ± 1.88%	1.68%	39 394 ± 3.40%	22.51%
ME-gPC ($\theta_1 = 4.8 \cdot 10^{-3}$ and $\theta_2 = 1\%$)	5 706	2.25 hours	53.13% ± 1.88%	1.68%	45 454 ± 3.33%	3.22%
ME-gPC ($\theta_1 = 3.5 \cdot 10^{-3}$ and $\theta_2 = 0.1\%$)	7 023	2.96 hours	52.34% ± 0.19%	0.35%	46 970 ± 3.22%%	0%

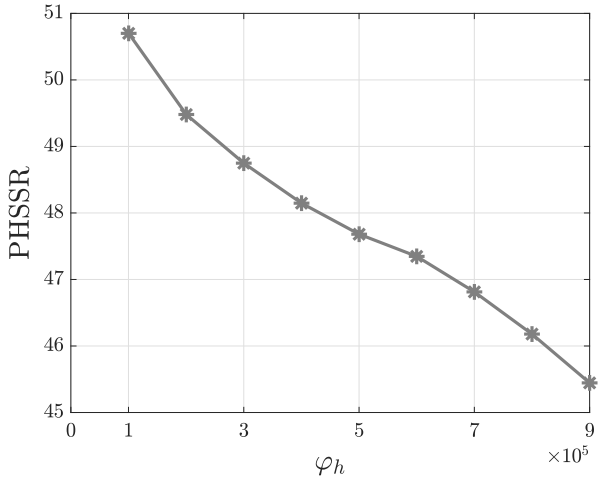

Figure 9: PHSSR as a function of φ_h for $\eta_h = 0.024$ and $\varphi_h \in [0\ 900\,000]$ N·kg^{-1}·m^{-3}. The mitigation limits are assessed using the reference method.

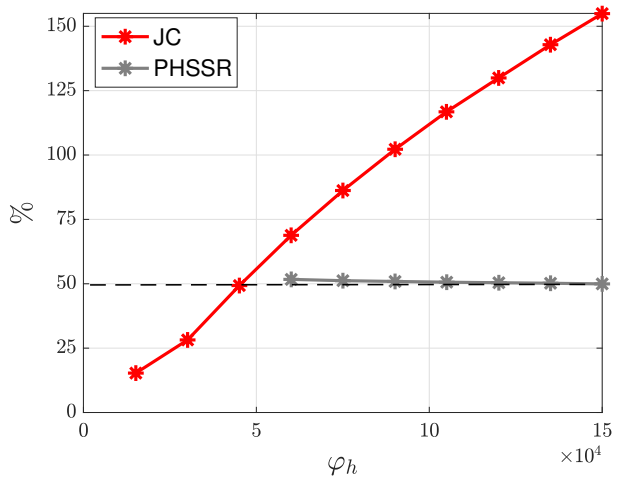

Figure 10: Evolutions of the Jump Criterion (JC) and of the PHSSR as functions of φ_h obtained with the reference method.

mum θ_1 value difficult. Another way to reduce the error levels is to increase the value of the precision threshold θ_2. The optimum value of the jump detection threshold θ_1 depending on the precision threshold θ_2, the optimum pair of thresholds is finally found as $\theta_1 = 3.5 \cdot 10^{-}3$ and $\theta_2 = 0.1$ %. The corresponding relative errors are 0.19 % for $\text{PHSSR}^{\max}$ and $Err = 0$ % for φ_h^{opt}, while the number of simulations has increased from 5706 to 7023. It is therefore observed that the precision level depends on the accepted computational cost. In this study, the final computational cost (7 023) with the ME-gPC method remains much weaker than that of the reference method (100 000). *Remark:* as in section 6.1 for the optimization of the NES damping coefficient, identical values of $\text{PHSSR}^{\max}$ may be observed with the ME-gPC method. The widths of the plateaus decrease when the precision threshold θ_1 is reduced.

7. Results for stochastic design variables

The second optimization technique considers that the NES parameters are also uncertain with a known probability law. Thus, the design variables to be optimized are not directly the NES parameters but one of their statistics called hyperparameters. In this work, the design parameters follow uniform probability distributions and the considered hyperparameter is the mean $\tilde{x}_d$. Regarding the

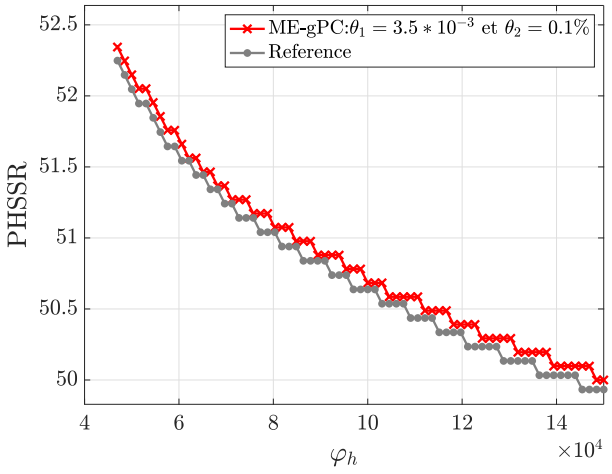

Figure 11: PHSSR as a function of φ_h for $\eta_h = 0.024$ and $\varphi_h \in [0\ 150\,000]$ N·kg^{-1}·m^{-3}. The thresholds are respectively: $\theta_1 = 3.5 \cdot 10^{-3}$ and $\theta_2 = 0.1\%$. The reference results are obtained as described in Sect. 6.2.2.

system parameters, as previously only the friction coefficient μ is assumed to be uncertain.

7.1. Optimization of the NES damping coefficient

7.1.1. Reference optimization

In this section, the optimization problem (18) is solved with a single design variable (hyperparameter) defined as the mean $\hat{\eta}_h$ of the NES damping coefficient η_h, which is a stochastic parameter following a uniform law. The NES cubic stiffness is fixed and equal to $\varphi_h = 140\ 000$ N·kg^{-1}·m^{-3}. The design space is divided into $N_I = 5$ intervals as shown in Tab. 3. For each interval the lower and upper bounds are determined as follows: $\eta_h^{\text{inf}} = \hat{\eta}_h - 0.1\hat{\eta}_h$ and $\eta_h^{\text{sup}} = \hat{\eta}_h + 0.1\hat{\eta}_h$ where $\hat{\eta}_h$ is the mean. The mean values are chosen so that the upper bound of one interval coincides with the lower bound of the next interval.

In each interval, $N_d = 10$ random samples of damping coefficient values η_h are drawn according to the uniform probability law. For each of these 10 samples, the mitigation limit and the PHSSR are determined directly from the numerical simulation of (2) using 10000 values of the friction coefficient μ. The objective function to be maximized is now the mean $\mathbf{E}$[PHSSR] of the 10 PHSSR values obtained in each interval.

Tab. 3 shows the reference results of the $\hat{\eta}_h$ optimization. For each interval, the mean of the 10 samples of η_h is calculated and compared to the theoretical $\hat{\eta}_h$ value in order to validate the number of samples. The mean PHSSR value $\mathbf{E}$[PHSSR] is also indicated, along with the error on $\mathbf{E}$[PHSSR] for a confidence level of 99%. The resulting values (errors lower than 0.15%) show that the number of samples $N_d = 10$ of η_h in each interval is sufficient.

Fig. 12 displays the evolutions of $\mathbf{E}$[PHSSR], PHSSR$^{\text{max}}$ and PHSSR$^{\text{min}}$ as functions of $\hat{\eta}_h$. In this case, the maximum value of the objective function is 50.07%, which corresponds to an optimal theoretical value of $\hat{\eta}_h$ equal to 0.0237. The number of simulations is equal to $5 \times 10 \times 10\,000 = 500\,000$.

7.1.2. Optimization with the ME-gPC method

Tab. 4 shows the results of the optimization of $\hat{\eta}_h$ by the ME-gpC based method. The gPC order is again chosen as $p = 1$, θ_1 is set to $1 \cdot 10^{-3}$ and two values of θ_2 are tested: $\theta_2 = 1\%$ and $\theta_2 = 0.001\%$. The design space is the same as for the reference optimization and the same quantities are considered.

Tab. 5 compares the results obtained with the three strategies (reference optimization and ME-gPC based optimizations with $\theta_2 = 1\%$ and $\theta_2 = 0.001\%$). The corresponding evolutions of $\mathbf{E}$[PHSSR], PHSSR$^{\text{max}}$ and PHSSR$^{\text{min}}$ according to $\hat{\eta}_h$ are displayed in Fig. 12.

In the case of $\theta_2 = 1\%$, the number of simulations is equal to 4613, leading to a computational cost reduction of 98.98%. The maximum value of the objective function is here 50.78%, which corresponds to the same optimal value $\hat{\eta}_h = 0.0237$ as for the reference case. The relative error of the maximum PHSSR mean value with respect to the reference is $E_{\mathbf{E}[\text{PHSSR}]^{\text{max}}} = 1.41\%$.

For $\theta_2 = 0.001\%$, the number of simulations is increased to 8006, which still induces a high computational cost reduction of 98.38%. The maximum value of the objective function is equal to that of the reference case, 50.07%, leading to a relative error $E_{\mathbf{E}[\text{PHSSR}]^{\text{max}}} = 0\%$. The corresponding optimal value of $\hat{\eta}_h$ is again equal to 0.0237.

As for the optimization with deterministic design variables, it is again shown that a proper choice of the precision threshold θ_2 enables the reduction of the error levels. However, an error reduction leads to an increase of the required simulation number (from 4613 to 8006), and thus the retained precision level depends on the accepted computational cost. In both cases presented above, the computational costs with the ME-gPC optimization remains much weaker than that of the reference method (500 000). Moreover, it can be noticed that the optimal values of the mean of η_h, $\hat{\eta}_h = 0.0237$, and of the PHSSR mean, $\mathbf{E}(\text{PHSSR}) = 50,07\%$, are the same as those obtained with the deterministic optimization. This result is logical because the curve of the PHSSR as a function of η_h varies very little around the optimal value. Thus, the PHSSR mean remains practically constant.

7.2. Optimization of the NES nonlinear stiffness

7.2.1. Reference optimization

The last optimization problem proposed in this paper (still represented by (18)) considers a single design variable (hyperparameter) $\hat{\varphi}_h$ which is here the mean of the NES nonlinear stiffness φ_h; similarly to the previous optimization problem, φ_h is a stochastic parameter supposed to follow a uniform law. The NES damping coefficient η_h is set to 0.024.

Table 3: Results of the reference optimization (see Sect. 7.1.1). The design parameter is $\hat{\eta}_h$.

$[\eta_h^{\inf}, \eta_h^{\sup}]$	Theoretical mean $\hat{\eta}_h$	Mean of the 10 samples of η_h	$\mathbf{E}$[PHSSR] (%)	Error on $\mathbf{E}$[PHSSR] for a confidence level = 99% (%)
[0.0117,0.0143]	0.0130	0.0129	48.36	0.1417
[0.0143,0.0175]	0.0159	0.0161	49.31	0.1086
[0.0175,0.0214]	0.0194	0.0193	48.85	0.0220
[0.0214,0.0261]	0.0237	0.0234	50.07	0.0005
[0.0261,0.0319]	0.0290	0.0284	49.90	0.0277

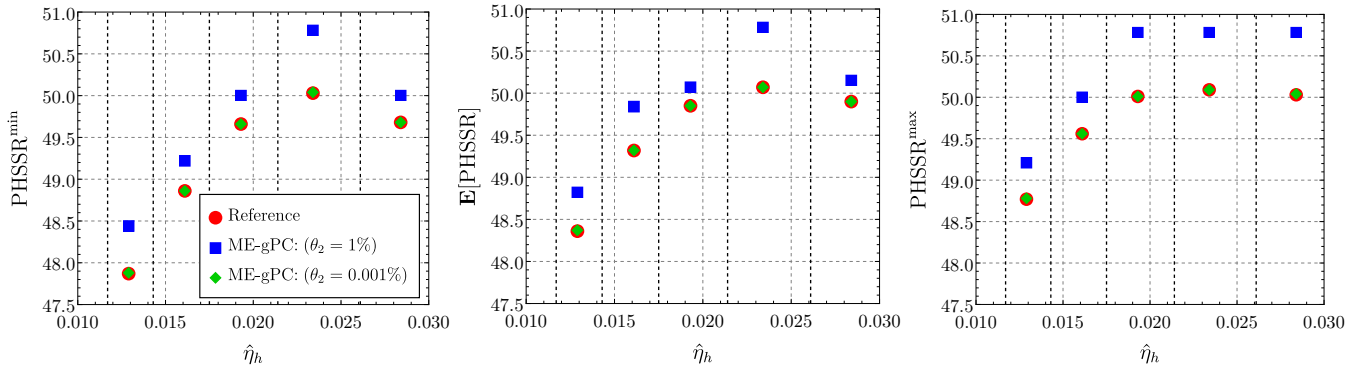

(a) Minimum of PHSSR (b) Mean of PHSSR (c) Maximum of PHSSR

Figure 12: Evolutions of $\mathbf{E}$[PHSSR], $\text{PHSSR}^{\max}$ and $\text{PHSSR}^{\min}$ as functions of $\hat{\eta}_h$ obtained with the reference method, the ME-gPC based method with θ_2 = 1 %, and the ME-gPC based method with θ_2 = 0.001 %. The black segments denote the limits of the intervals. The reference results are obtained as described in Sect. 7.1.1.

Table 4: Results of the optimization with the ME-gPC method. The design parameter is $\hat{\eta}_h$.

			θ_2 = 1 %		θ_2 = 0.001 %	
$[\eta_h^{\inf}, \eta_h^{\sup}]$	Theoretical mean	Mean of the 10 samples of η_h	$\mathbf{E}$[PHSSR] (%)	Error on $\mathbf{E}$[PHSSR] for a confidence level = 99% (%)	$\mathbf{E}$[PHSSR] (%)	Error on $\mathbf{E}$[PHSSR] for a confidence level = 99% (%)
[0.0117,0.0143]	0.0130	0.0129	48.82	0.2833	48.37	0.1423
[0.0143,0.0175]	0.0159	0.0161	49.84	0.1776	49.32	0.1091
[0.0175,0.0214]	0.0194	0.0193	50.07	0.0994	49.85	0.0224
[0.0214,0.0261]	0.0237	0.0234	50.78	0	50.07	0.0005
[0.0261,0.0319]	0.0290	0.0284	50.15	0.1765	49.90	0.0280

The methodology is similar to that of the previous section with a design space divided into N_I = 5 intervals as shown in Tab. 6. The lower and upper bounds of the intervals are again defined as $\varphi_h^{\inf} = \hat{\varphi}_h - 0.1\hat{\varphi}_h$ and $\varphi_h^{\sup} = \hat{\varphi}_h + 0.1\hat{\varphi}_h$, where the mean value $\hat{\varphi}_h$ is chosen so that the upper bound of one interval coincides with the lower bound of the next interval.

As previously, N_d = 10 random samples of stiffness values φ_h are drawn in each interval according to the uniform probability law, and for each sample the mitigation limit and the PHSSR are directly determined from the numerical simulation of (2) using 10000 values of the friction coefficient μ. The objective function to be maximized is the mean $\mathbf{E}$[PHSSR] of the 10 PHSSR values obtained in each interval.

In section 6.2 it has been shown that the PHSSR is a decreasing function of φ_h, which implies that the optimal value is the lowest value of φ_h for which the jump criterion (16) is met. It is therefore possible that a part of the interval where this optimal value lies (in concrete terms here, some of the 10 samples in the first interval [38 438, 46 980] $\text{N}\cdot\text{kg}^{-1}\cdot\text{m}^{-3}$) corresponds to φ_h values for which the jump criterion (16) is not respected. In that case, 10 new samples of φ_h values are generated in the part of the interval

Table 5: Comparison between the reference optimization and the ME-gPC based optimization. The design parameter is $\hat{\eta}_h$. The reference results are obtained as described in Sect. 7.1.1.

	Nb of simulations	Computational time	Computational cost reduction(%)	$\mathbf{E}[\text{PHSSR}]^{\max}$	$E_{\mathbf{E}[\text{PHSSR}]^{\max}}$	$\hat{\eta}_h^{\text{opt}}$
Reference	500 000	7.86 days	-	50.07% ± 0.02%	–	0.0237
ME-gPC ($\theta_1 = 1 \cdot 10^{-3}$ and $\theta_2 = 1\%$)	4 613	1.92 hours	98.98	50.78% ± 2%	1.41%	0.0237
ME-gPC ($\theta_1 = 1 \cdot 10^{-3}$ and $\theta_2 = 0.001\%$)	8 006	3.29 hours	98.38	50.07% ± 0.02%	0%	0.0237

(here [38 438, 46 980]) for which (16) is satisfied.

Tab. 6 shows the reference results of the $\hat{\varphi}_h$ optimization. Similarly to the previous section, the mean of the 10 samples φ_h is calculated for each interval and compared to the theoretical $\hat{\varphi}_h$ value. The mean value $\mathbf{E}$[PHSSR] is also indicated, along with the error on $\mathbf{E}$[PHSSR] for a confidence level of 99%. With very low error levels (lower than 0.03%), the number of φ_h samples $N_d = 10$ in each interval is again found sufficient. This reference optimization has required a simulation number equal to $5 \times 10 \times 10\,000 = 500\,000$.

The evolutions of $\mathbf{E}$[PHSSR], $\text{PHSSR}^{\max}$ and $\text{PHSSR}^{\min}$ according to $\hat{\varphi}_h$ are displayed in Fig. 13. In this case, the maximum value of the objective function is 52.32% which corresponds to an optimal value of $\hat{\varphi}_h$ equal to 46678. The very low error on the E(PHSSR) for a 99% confidence level obtained in this case is due to the fact that the PHSSR values are close in the interval.

7.2.2. Optimization with the ME-gPC method

Tab. 7 shows the results of the optimization of $\hat{\varphi}_h$ based on the ME-gPC, with again a gPC order $p = 1$, $\theta_1 = 4.8 \cdot 10^{-3}$ and two values of θ_2: $\theta_2 = 1\%$ and $\theta_2 = 0.001\%$. The design space is discretized as for the reference optimization. For several intervals the error on $\mathbf{E}$[PHSSR] for a confidence level of 99% is null, meaning that the 10 PHSSR values corresponding to the 10 samples are identical. The evolutions of $\mathbf{E}$[PHSSR], $\text{PHSSR}^{\max}$ and $\text{PHSSR}^{\min}$ according to $\hat{\varphi}_h$ for the cases $\theta_2 = 1\%$ and $\theta_2 = 0.001\%$ are visible in Fig. 13 along with the reference results.

The comparison of the different strategies to optimize the NES nonlinear stiffness (that is, the reference optimization and the two ME-gPC based optimizations with $\theta_2 = 1\%$ and $\theta_2 = 0.001\%$) is presented in Tab. 8. In the case of $\theta_1 = 4.8 \cdot 10^{-3}$ and $\theta_2 = 1\%$, the number of simulations is equal to 3248, leading to a computational cost reduction of 99.21%. The maximum value of the objective function is 52.73%, which corresponds to an optimal value of $\hat{\varphi}_h$ equal to 46 678 $\text{N}\cdot\text{kg}^{-1}\cdot\text{m}^{-3}$, and the relative error on the maximum value of the PHSSR mean is $E_{\mathbf{E}[\text{PHSSR}]^{\max}} = 1.5\%$.

When $\theta_1 = 2 \cdot 10^{-3}$ and $\theta_2 = 0.001\%$, the number of simulations is increased up to 6947, inducing a slightly reduced computational cost reduction of 98.30%. The maximum value of the objective function is now 52.33%, the optimal value of $\hat{\varphi}_h$ 46 678 $\text{N}\cdot\text{kg}^{-1}\cdot\text{m}^{-3}$, and the relative error on the maximum value of the PHSSR mean $E_{\mathbf{E}[\text{PHSSR}]^{\max}} = 0.09\%$.

The conclusions given for the optimization of the damping coefficient with the ME-gPC based method hold here: the choice of the precision threshold θ_2 enables the control of the error levels but impacts the computational costs, which remain however much lower than that with the reference method (500 000 simulations).

8. Conclusion

In this paper, the robust optimization of NES used to mitigate limit cycles of a friction system with an uncertain friction coefficient has been studied. The optimization strategy is based on the maximization of the propensity of the system to be in an attenuated regime (PHSSR), which constitutes the objective function of the problem. Two original approaches are proposed, depending on whether the parameters of the NES are considered as deterministic or as uncertain, but with a known probability distribution. In each case, two optimization strategies are developed, that consist in evaluating the objective function by either a deterministic reference optimization or by a method based on the Multi-Element generalized Polynomial Chaos (the so-called ME-gPC method). The comparison between the two methods shows the efficiency of the ME-gPC method to significantly reduce the computational cost while keeping a good accuracy compared to the reference optimization.

These optimization approaches have been applied to determine the optimal values of the NES parameters to maximize their ability to passively attenuate limit cycle of oscillations. Concerning the NES nonlinear stiffness, the optimal value is the lowest value for which the discontinuity jump is considered as high enough. Concerning

Table 6: Results of the reference optimization (see Sect. 7.2.1). The design parameter is $\hat{\varphi}_h$.

	Theoretical mean $\hat{\varphi}_h$	Mean of 10 samples of φ_h	$\mathbf{E}$[PHSSR] (%)	Error on $\mathbf{E}$[PHSSR] for a confidence level = 99% (%)
[38 438, 46 980]	42 709	46 678	52.32	0.0004
[46 980, 57 420]	52 200	52 992	51.95	0.0299
[57 420, 70 180]	63 800	62 746	51.53	0.0296
[70 180, 85 776]	77 978	78 942	51.07	0.0095
[85 776, 104 837]	95 306	94 876	50.76	0.0200

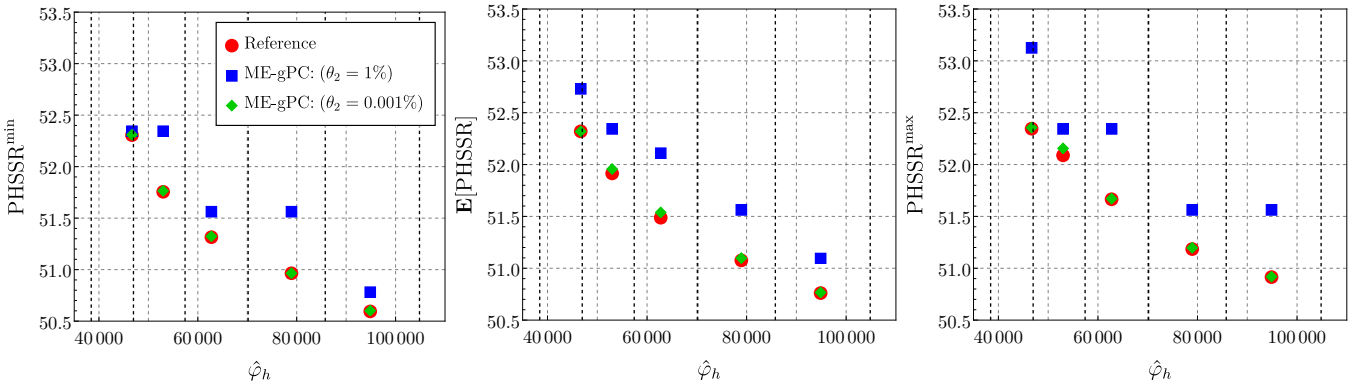

(a) Minimum of PHSSR (b) Mean of PHSSR (c) Maximum of PHSSR

Figure 13: Evolutions of $\mathbf{E}$[PHSSR], $\text{PHSSR}^{\max}$ and $\text{PHSSR}^{\min}$ as functions of $\hat{\varphi}_h$ with the reference method, the ME-gPC based method with $\theta_2 = 1$ % and the ME-gPC based method with $\theta_2 = 0.001$ %. The black segments denote the limits of the intervals. The reference results are obtained as described in Sect. 7.2.1.

Table 7: Results of the optimization with the ME-gPC method. The design parameter is $\hat{\varphi}_h$.

			$\theta_2 = 1$ %		$\theta_2 = 0.001$ %	
$[\varphi_h^{\inf}, \varphi_h^{\sup}]$	Theoretical mean $\hat{\varphi}_h$	Mean of the 10 samples of φ_h	$\mathbf{E}$[PHSSR] (%)	Error on $\mathbf{E}$[PHSSR] for a confidence level = 99% (%)	$\mathbf{E}$[PHSSR] (%)	Error on $\mathbf{E}$[PHSSR] for a confidence level = 99% (%)
[38 438, 46 980]	42 709	46 678	52.73	0.4721	52.33	0.0007
[46 980, 57 420]	52 200	52 992	52.34	0	51.91	0.0148
[57 420, 70 180]	63 800	62 746	52.10	0.2230	51.48	0.0399
[70 180, 85 776]	77 978	78 942	51.56	0	51.09	0.0105
[85 776, 104 837]	95 306	94 876	51.09	0.2599	50.76	0.0206

the NES damping coefficient, the curve representing the PHSSR as a function of the damping coefficient is nonlinear and presents a maximum corresponding to the optimal NES damping value. However, the variations of the PHSSR near the optimal value are very small, which makes it more difficult (but also less crucial) to precisely locate this optimal value.

The general nature of the proposed strategy suggests that it could be used for the robust optimization of any vibration absorber, providing that the transition from the attenuated state to the non-attenuated state passes through a discontinuity in the amplitude profile of the system as a function of the bifurcation parameter considered.

In future works, several issues should be tackled. First, as one of the difficulties of the proposed approach is to choose relevant values for the thresholds, it could be interesting to develop automatically adaptive thresholds. Another issue lies in the extension of the proposed method to several uncertain parameters. It can also be envisaged to study the efficiency of the method for a model with a higher number of degrees of freedom.

Table 8: Comparison between the reference optimization and the optimization with the ME-gPC method. The design parameter is $\hat{\varphi}_h$. The reference results are obtained as described in Sect. 7.2.1.

	Nb of simulations	Computational time	Computational cost reduction (%)	$\mathbf{E}[\text{PHSSR}]^{\max}$	$E_{\mathbf{E}[\text{PHSSR}]^{\max}}$	$\hat{\varphi}_h^{\text{opt}}$
Reference	500 000	7.53 days	-	$52.32\% \pm 0.02\%$	–	46 678
ME-gPC ($\theta_1 = 4.8 \cdot 10^{-3}$ and $\theta_2 = 1\%$)	3248	1.42 hours	99.21	$52.73\% \pm 1.9\%$	1.50%	46 678
ME-gPC ($\theta_1 = 2 \cdot 10^{-3}$ and $\theta_2 = 0.001\%$)	6947	3.06 hours	98.30	$52.33\% \pm 0.019\%$	0.09%	46 678

References

Askey, R., Wilson, J., 1985. Some basic hypergeometric orthogonal polynomials that generalize Jacobi polynomials. volume 319. American Mathematical Soc.

Bergeot, B., 2021. Scaling law for the slow flow of an unstable mechanical system coupled to a nonlinear energy sink. Journal of Sound and Vibration 503, 116109. URL: https://doi.org/10.1016/j.jsv.2021.116109, doi:10.1016/j.jsv.2021.116109.

Bergeot, B., Bellizzi, S., Berger, S., 2020. Dynamic behavior analysis of a mechanical system with two unstable modes coupled to a single nonlinear energy sink. Communications in Nonlinear Science and Numerical Simulation 95, 105623. URL: https://doi.org/10.1016/j.cnsns.2020.105623, doi:10.1016/j.cnsns.2020.105623.

Bergeot, B., Berger, S., Bellizzi, S., 2017. Mode coupling instability mitigation in friction systems by means of nonlinear energy sinks : numerical highlighting and local stability analysis. Journal of Vibration and Control 24, 3487–3511. doi:10.1177/1077546317707101.

Berveiller, M., Sudret, B., Lemaire, M., 2006. Stochastic finite element: a non intrusive approach by regression. European Journal of Computational Mechanics/Revue Européenne de Mécanique Numérique 15, 81–92.

Boroson, E., Missoum, S., Mattei, P.O., Vergez, C., 2017. Optimization under uncertainty of parallel nonlinear energy sinks. Journal of Sound and Vibration 394, 451–464. URL: http://linkinghub.elsevier.com/retrieve/pii/S0022460X16308045, doi:10.1016/j.jsv.2016.12.043.

Boroson, E.R., 2015. Optimization under uncertainty of nonlinear energy sinks. URL: http://hdl.handle.net/10150/595972.

Cameron, R., Martin, W., 1947. The orthogonal development of nonlinear functionals in series of fourier-hermite functionals. Annals of Mathematics 48, 385–392. doi:http://dx.doi.org/10.2307/1969178.

Fang, S., Chen, K., Xing, J., Zhou, S., Liao, W.H., 2021. Tuned bistable nonlinear energy sink for simultaneously improved vibration suppression and energy harvesting. International Journal of Mechanical Sciences 212, 106838. URL: https://www.sciencedirect.com/science/article/pii/S0020740321005610, doi:https://doi.org/10.1016/j.ijmecsci.2021.106838.

Fritz, G., Sinou, J.J., Duffal, J.M., Jézéquel, L., 2007. Investigation of the relationship between damping and mode-coupling patterns in case of brake squeal. Journal of Sound and Vibration 307, 591–609. doi:10.1016/j.jsv.2007.06.041.

Geng, X.F., Ding, H., Mao, X.Y., Chen, L.Q., 2021. Nonlinear energy sink with limited vibration amplitude. Mechanical Systems and Signal Processing 156, 107625. URL: https://www.sciencedirect.com/science/article/pii/S0888327021000200, doi:https://doi.org/10.1016/j.ymssp.2021.107625.

Habib, G., Romeo, F., 2021. Tracking modal interactions in nonlinear energy sink dynamics via high-dimensional invariant manifold. Nonlinear Dynamics 103, 3187–3208. URL: https://doi.org/10.1007/s11071-020-05937-4, doi:10.1007/s11071-020-05937-4.

Hervé, B., Sinou, J.J., Mahé, H., Jézéquel, L., 2008. Analysis of squeal noise and mode coupling instabilities including damping and gyroscopic effects. European Journal of Mechanics - A/Solids 27, 141–160. URL: http://www.sciencedirect.com/science/article/pii/S0997753807000447, doi:10.1016/j.euromechsol.2007.05.004.

Hultén, J., 1993. Brake squeal - a self-exciting mechanism with constant friction, in: SAE Truck and Bus Meeting, Detroit, Mi, USA.

Hultén, J., 1997. Friction phenomena related to drum brake squeal instabilities, in: ASME Design Engineering Technical Conferences, Sacramento, CA.

Karama, M., Hamdi, M., Habbad, M., 2021. Energy harvesting in a nonlinear energy sink absorber using delayed resonators. Nonlinear Dynamics 105, 113–129. URL: https://doi.org/10.1007/s11071-021-06611-z, doi:10.1007/s11071-021-06611-z.

Karličić, D., Cajić, M., Paunović, S., Adhikari, S., 2021. Periodic response of a nonlinear axially moving beam with a nonlinear energy sink and piezoelectric attachment. International Journal of Mechanical Sciences 195. doi:10.1016/j.ijmecsci.2020.106230.

Khazaee, M., Khadem, S., Moslemi, A., Abdollahi, A., 2019. A comparative study on optimization of multiple essentially nonlinear isolators attached to a pipe conveying fluid. Mechanical Systems and Signal Processing , 106442URL: http://www.sciencedirect.com/science/article/pii/S0888327019306636, doi:https://doi.org/10.1016/j.ymssp.2019.106442.

Lee, Y.S., Vakakis, A.F., Bergman, L.A., McFarland, D.M., 2006. Suppression of limit cycle oscillations in the van der Pol oscillator by means of passive non-linear energy sinks. Structural Control and Health Monitoring 13, 41–75. doi:10.1002/stc.143.

Li, H., Li, A., 2021. Potential of a vibro-impact nonlinear energy sink for energy harvesting. Mechanical Systems and Signal Processing 159, 107827. URL: https://www.sciencedirect.com/science/article/pii/S0888327021002223, doi:https://doi.org/10.1016/j.ymssp.2021.107827.

McKay, M., Beckman, R., Conover, W., 1979. A comparison of three methods for selecting values of input variables in the analysis of output from a computer code. Technometrics 21, 239–245. URL: http://www.jstor.org/stable/1268522, doi:10.2307/1268522.

Nechak, L., Berger, S., Aubry, E., 2011. A polynomial chaos approach to the robust analysis of the dynamic behaviour of friction systems. European Journal of Mechanics - A/Solids 30, 594 – 607. URL: http://www.sciencedirect.com/science/article/pii/S0997753811000258, doi:https://doi.org/10.1016/j.euromechsol.2011.03.002.

Nechak, L., Berger, S., Aubry, E., 2012. Prediction of random self friction-induced vibrations in uncertain dry friction systems using

a multi-element generalized polynomial chaos approach. Journal of Vibration and Acoustics 134, 041015. URL: http://dx.doi.org/10.1115/1.4006413, doi:10.1115/1.4006413.

Nechak, L., Berger, S., Aubry, E., 2013. Non-intrusive generalized polynomial chaos for the robust stability analysis of uncertain nonlinear dynamic friction systems. Journal of Sound and Vibration 332, 1204 – 1215. URL: http://www.sciencedirect.com/science/article/pii/S0022460X12008462, doi:http://dx.doi.org/10.1016/j.jsv.2012.09.046.

Nechak, L., Besset, S., Sinou, J.J., 2018. Robustness of stochastic expansions for the stability of uncertain nonlinear dynamical systems – application to brake squeal. Mechanical Systems and Signal Processing 111, 194 – 209. URL: http://www.sciencedirect.com/science/article/pii/S0888327018300293, doi:https://doi.org/10.1016/j.ymssp.2018.01.021.

Nguyen, T.A., Pernot, S., 2011. Design criteria for optimally tuned nonlinear energy sinks—part 1: transient regime. Nonlinear Dynamics 69, 1–19. doi:10.1007/s11071-011-0242-9.

Nouy, A., 2009. Recent developments in spectral stochastic methods for the numerical solution of stochastic partial differential equations. Archives of Computational Methods in Engineering 16, 251–285. doi:10.1007/s11831-009-9034-5.

Oden, J., Martins, J., 1985. Models and computational methods for dynamic friction phenomena. Computer Methods in Applied Mechanics and Engineering 52, 527–634. doi:10.1016/0045-7825(85)90009-X.

Oliva, M., Barone, G., Navarra, G., 2017. Optimal design of nonlinear energy sinks for {SDOF} structures subjected to white noise base excitations. Engineering Structures 145, 135 – 152. URL: http://www.sciencedirect.com/science/article/pii/S014102961730888X, doi:https://doi.org/10.1016/j.engstruct.2017.03.027.

Pidaparthi, B., Missoum, S., 2018. Optimization of nonlinear energy sinks for the mitigation of limit cycle oscillations, in: 2018 Multidisciplinary Analysis and Optimization Conference, American Institute of Aeronautics and Astronautics. doi:10.2514/6.2018-3569.

Pidaparthi, B., Missoum, S., 2019. Stochastic optimization of nonlinear energy sinks for the mitigation of limit cycle oscillations. AIAA Journal , 1–11doi:10.2514/1.j057897.

Qiu, D., Seguy, S., Paredes, M., 2019. Design criteria for optimally tuned vibro-impact nonlinear energy sink. Journal of Sound and Vibration 442, 497 – 513. URL: http://www.sciencedirect.com/science/article/pii/S0022460X18307831, doi:https://doi.org/10.1016/j.jsv.2018.11.021.

Sarrouy, E., Dessombz, O., Sinou, J.J., 2012. Stochastic analysis of the eigenvalue problem for mechanical systems using polynomial chaos expansion— application to a finite element rotor. Journal of Vibration and Acoustics 134. doi:10.1115/1.4005842.

Sarrouy, E., Dessombz, O., Sinou, J.J., 2013. Stochastic study of a non-linear self-excited system with friction. European Journal of Mechanics-A/Solids 40, 1–10.

Snoun, C., Bergeot, B., Berger, S., 2020. Prediction of the dynamic behavior of an uncertain friction system coupled to nonlinear energy sinks using a multi-element generalized polynomial chaos approach. European Journal of Mechanics - A/Solids 80, 103917. URL: http://www.sciencedirect.com/science/article/pii/S0997753819307132, doi:https://doi.org/10.1016/j.euromechsol.2019.103917.

Tian, W., Zhao, T., Gu, Y., Yang, Z., 2021. Nonlinear flutter suppression and performance evaluation of periodically embedded nonlinear vibration absorbers in a supersonic FGM plate. Aerospace Science and Technology 1, 107198. URL: https://doi.org/10.1016/j.ast.2021.107198, doi:10.1016/j.ast.2021.107198.

Trinh, M., Berger, S., Aubry, E., 2016. Stability analysis of a clutch system with multi-element generalized polynomial chaos. Mechanics & Industry 17, 205. URL: https://doi.org/10.1051/meca/2015061, doi:10.1051/meca/2015061.

Vakakis, A., Gendelman, O., 2001. Energy pumping in nonlinear mechanical oscillators: Part II - Resonance capture. Journal of Applied Mechanics 68, 42–48.

Vakatis, A.F., Gendelman, O.V., Bergman, L.A., McFarland, D.M., Kerschen, G., Lee, Y.S., 2008. Nonlinear Targeted Energy Transfer in Mechanical and Structural Systems. Springer-Verlag, Berlin, New York.

Wan, X., Karniadakis, G.E., 2005. An adaptive multi-element generalized polynomial chaos method for stochastic differential equations. Journal of Computational Physics 209, 617 – 642. URL: http://www.sciencedirect.com/science/article/pii/S0021999105001919, doi:https://doi.org/10.1016/j.jcp.2005.03.023.

Wang, J., Wierschem, N.E., Wang, B., Spencer, B.F., 2019. Multi-objective design and performance investigation of a high-rise building with track nonlinear energy sinks. The Structural Design of Tall and Special Buildings doi:10.1002/tal.1692.

Wiener, N., 1938. The homogeneous chaos. American Journal of Mathematics 60, 897. doi:10.2307/2371268.

Xiong, L., Tang, L., Liu, K., Mace, B.R., 2021. Effect of Electromechanical Coupling on Dynamic Characteristics of a Piezoelectric Nonlinear Energy Sink System. Journal of Vibration Engineering and Technologies 9, 687–699. URL: https://doi.org/10.1007/s42417-020-00255-w, doi:10.1007/s42417-020-00255-w.

Xiu, D., Karniadakis, G., 2002. The wiener–askey polynomial chaos for stochastic differential equations. SIAM Journal on Scientific Computing 24, 619–644. URL: http://dx.doi.org/10.1137/S1064827501387826, doi:10.1137/S1064827501387826, arXiv:http://dx.doi.org/10.1137/S1064827501387826.

Zhou, B., Thouverez, F., Lenoir, D., 2014. Essentially nonlinear piezoelectric shunt circuits applied to mistuned bladed disks. Journal of Sound and Vibration 333, 2520–2542. URL: http://dx.doi.org/10.1016/j.jsv.2013.12.019, doi:10.1016/j.jsv.2013.12.019.